

Parallel Gate Operations Fidelity in a Linear Array of Flip-Flop Qubits

Daive Rei, Elena Ferraro,* and Marco De Michielis*


Quantum computers based on silicon are promising candidates for long term universal quantum computation due to the long coherence times of electron and nuclear spin states. Furthermore, the continuous progress of micro- and nano-electronics, also related to the scaling of metal–oxide–semiconductor systems, makes it possible to control the displacement of single dopants thus suggesting their exploitation as qubit holders. Flip-flop qubit is a donor based qubit where interactions between qubits are achievable for distance up to several hundred nanometers. In this work, a linear array of flip-flop qubits is considered and the unwanted mutual qubit interactions due to the simultaneous application of two one-qubit and two two-qubit gates are included in the quantum gate simulations. In particular, by studying the parallel execution of couples of one-qubit gates, namely $R_z(-\frac{\pi}{2})$ and $R_x(-\frac{\pi}{2})$, and of couples of two-qubit gate, that is, \sqrt{i} SWAP, a safe inter-qubit distance is found where unwanted qubit interactions are negligible thus leading to parallel gates fidelity up to 99.9%.

1. Introduction

Donor atoms in silicon represent a well-known system to host qubits due to their potential for scalability and affinity with metal–oxide–semiconductor (MOS) technology, the transistor reference technology. This kind of qubit was proposed by Kane in 1998 where the nuclear spin states of a phosphorus donor atom into a silicon bulk define the qubit.^[1] The physical properties of this system are well known because are commonly used in semiconductor industry making silicon a promising candidate to realize a solid state quantum computer.

Moreover, silicon offers a long coherence time of electron and nuclear spin states and, in particular, its isotope ^{28}Si is spin-free, so the interactions between the spins of donor and silicon bulk, which compromise the coherence states of qubits system, are avoided.^[2–7]

D. Rei, E. Ferraro, M. De Michielis
CNR-IMM Agrate Unit
Via C. Olivetti 2, Agrate Brianza, Monza e Brianza 20864, Italy
E-mail: elena.ferraro@mdm.imm.cnr.it; marco.demichielis@mdm.imm.cnr.it

 The ORCID identification number(s) for the author(s) of this article can be found under <https://doi.org/10.1002/qute.202100133>

© 2022 The Authors. Advanced Quantum Technologies published by Wiley-VCH GmbH. This is an open access article under the terms of the Creative Commons Attribution License, which permits use, distribution and reproduction in any medium, provided the original work is properly cited.

DOI: 10.1002/qute.202100133

The realization of a two-qubit operation, which requires an interaction between qubits, is needed to implement a quantum algorithm. The interaction exploited in the Kane's qubit is the exchange interaction, that acting on a short range imposes an accurate donor placement. This circumstance represents one of the main issue related to the realization of this architecture.

Recently, the flip-flop qubit, a particular type of donor qubit, has been studied to overcome this limitation.^[8–11] It is constituted by a phosphorus donor atom embedded in a ^{28}Si substrate displaced at a distance d from a SiO_2 interface. At the top, a metal gate generates an electric field E_z to control the donor-bound electron position between the nucleus and the interface with the oxide. In this way, not only it is possible to define a qubit but also an electric dipole is created by the negatively charged

electron and the positively charged donor nucleus. Taking advantage of the dipole–dipole interaction, it enables the coupling between two qubits up to distances of an order of magnitude higher than the Kane's qubit, in the 100–500 nm range. The feature related to the long-distance interaction between two qubits relaxes the fabrication accuracy on metal gates and ^{31}P donors position needed to scale up the system. The interconnection between qubits is eased and the formation of a logical qubit, that is a system of more physical qubits which state is used to encode the state of a qubit, can be performed to protect the information by exploiting quantum error correction (QEC) codes.^[12] Depending on the QEC codes, logical gates can be simply obtained by applying the same operation to each physical qubit, that is, in a bit-wise fashion. Those logical gates can be greatly speeded up by fully exploiting gate parallelism. In order to take fully advantage of it, the effects of unwanted interactions between flip-flop qubits manipulated with the same gate in parallel need to be studied.

A universal quantum computer requires indeed the capability of performing single-qubit gates and two-qubit entangling operations in parallel.^[13,14] Study about quantum gate parallelism have been carried out on superconducting circuits,^[15] chains of atoms,^[14,16–18] and spins.^[13] In this work we address this kind of study on a linear array of flip-flop qubit.

The paper is organized as follows. In Section 2 the one-qubit system Hamiltonian and the definition of the flip-flop qubit states are introduced. Then, in Sections 3 and 4, studying the states evolution during the interaction with the external control electric field, different one-qubit gates, namely $R_z(-\frac{\pi}{2})$, $R_x(-\frac{\pi}{2})$ and a two-qubit operation, that is, the entangling \sqrt{i} SWAP gate, are

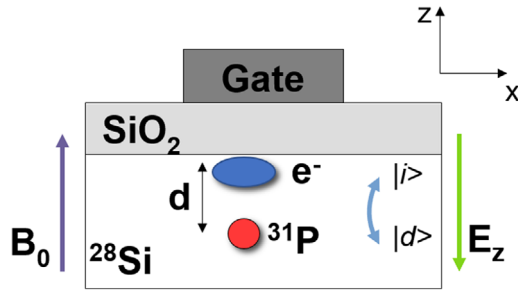


Figure 1. Flip-flop qubit scheme. A donor atom of ^{31}P is embedded in a bulk of ^{28}Si at a distance d from the Si/SiO₂ interface. Applying an electric field E_z through the metal gate, the electron position between the nucleus ($|d\rangle$) and the interface ($|i\rangle$) with the dielectric is controlled. A constant magnetic field B_0 is also applied along the z -axis.

presented and the study of the gate fidelity in presence of $1/f$ noise for these operations applied in parallel between two qubits and two couples of qubits is investigated. Finally, in Section 5 the conclusions of this work are provided.

2. Flip-Flop Qubit

The flip-flop qubit is described in the 8D Hilbert space that takes into account the spin states of the donor electron (nucleus) $\{|\downarrow\rangle; |\uparrow\rangle\}$ ($\{|\psi\rangle; |\uparrow\rangle\}$) and the orbital degree of freedoms $\{|g\rangle; |e\rangle\}$. The energy difference between the electron ground $|g\rangle$ and excited $|e\rangle$ states is given by^[8,19]

$$\epsilon_0 = \sqrt{V_t^2 + \left(\frac{d e(E_z - E_z^0)}{h}\right)^2} \quad (1)$$

where $E_z - E_z^0 \equiv \Delta E_z$ is the difference between the vertical electric field E_z applied by the gate and its value E_z^0 at the ionization point, where the electron is shared halfway between donor and interface. V_t is the tunnel coupling between the donor and the interface potential wells, e is the elementary charge, h is the Planck constant and d is the distance between the nucleus and the interface. A flip-flop qubit scheme is reported in **Figure 1**.

The Hamiltonian \hat{H} describing the flip-flop qubit is composed by the Zeeman part \hat{H}_{B_0} , the hyperfine coupling term \hat{H}_A and the orbital part \hat{H}_{Orb} ^[8]

$$\hat{H} = \hat{H}_{B_0} + \hat{H}_A + \hat{H}_{\text{Orb}} \quad (2)$$

Each term can be written as a function of the Pauli matrices

$$\hat{\sigma}_z = |g\rangle\langle g| - |e\rangle\langle e| \quad (3)$$

$$\hat{\sigma}_x = |g\rangle\langle e| + |e\rangle\langle g| \quad (4)$$

and the electron (nuclear) spin operators \mathbf{S} (\mathbf{I}), with \hat{z} component \hat{S}_z (\hat{I}_z).

The first two terms \hat{H}_{B_0} and \hat{H}_A which have the following expressions

$$\hat{H}_{B_0} = \gamma_e B_0 \left[\hat{1} + \left(\frac{\hat{1}}{2} + \frac{d e \Delta E_z}{2 h \epsilon_0} \hat{\sigma}_z + \frac{V_t}{2 \epsilon_0} \hat{\sigma}_x \right) \Delta_\gamma \right] \hat{S}_z - \gamma_n B_0 \hat{I}_z \quad (5)$$

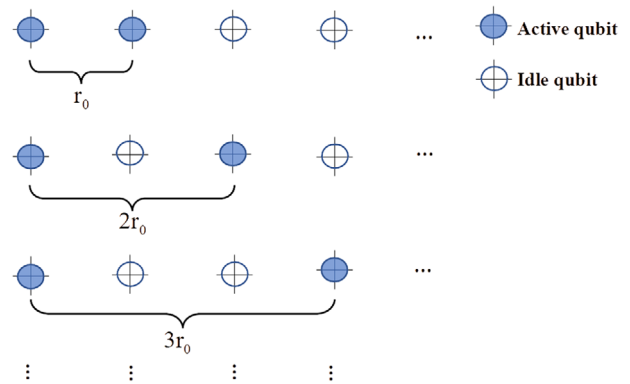


Figure 2. Scheme of a linear array of flip-flop qubits in three different example configurations. Each qubit is positioned at a distance r_0 from the adjacent one and two parallel one-qubit operations are executed on qubits displaced by a distance r , multiple of r_0 . Qubits between active ones are assumed in idle.

$$\hat{H}_A = A \left(\frac{\hat{1}}{2} - \frac{d e \Delta E_z}{2 h \epsilon_0} \hat{\sigma}_z - \frac{V_t}{2 \epsilon_0} \hat{\sigma}_x \right) \mathbf{S} \cdot \mathbf{I} \quad (6)$$

describe the Zeeman splitting caused by a constant magnetic field B_0 and the hyperfine interaction, respectively. In particular, in Equation (5), Δ_γ takes into account the variation of the electron gyromagnetic ratio γ_e between the nucleus (27.97 GHz T^{-1}) and the interface, while $\gamma_n = 17.23 \text{ MHz T}^{-1}$ is the constant nuclear gyromagnetic ratio. The hyperfine coupling A is a function of the vertical electric field E_z applied by the gate and, in order to obtain its functional form, the results reported in ref. [8] are fitted with the function $A_0/(1 + \exp(c \Delta E_z))$, where $A_0 = 117 \text{ MHz}$ is the bulk value of A , obtaining the fit parameter $c = 5.174 \times 10^{-4} \text{ m V}^{-1}$.^[11] Finally, the operator $\hat{1}$ is the identity matrix.

The orbital part \hat{H}_{Orb} , which gives a treatment of the electron position between the interface and the donor as a two level system allowing a full quantum mechanical description of the system, is given by

$$\hat{H}_{\text{Orb}} = -\frac{\epsilon_0}{2} \hat{\sigma}_z - \frac{d e E_{\text{ac}}(t) \cos(\omega_E t + \phi)}{2 h} \left(\frac{d e \Delta E_z}{h \epsilon_0} \hat{\sigma}_z + \frac{V_t}{\epsilon_0} \hat{\sigma}_x \right) \quad (7)$$

where $E_{\text{ac}}(t)$ is the time dependent amplitude of an oscillating electric field with pulsation ω_E and phase ϕ .

The qubit states are defined as the tensor product between the electron ground state and the flip-flop antiparallel states, that is, $|0\rangle \equiv |g \downarrow \uparrow\rangle$ and $|1\rangle \equiv |g \uparrow \downarrow\rangle$.

For the study of the quantum operations carried out in the next sections the parameters reported in ref. [8] are used, that is, $B_0 = 0.4 \text{ T}$, $\Delta_\gamma = -0.002$, and $d = 15 \text{ nm}$.

3. Parallel One-Qubit Gates

In this section the focus is on the effects of the unwanted interactions between two qubits in a linear array operated with one-qubit gates in parallel. The two qubits are displaced at an inter-qubit distance r , where r is an integer multiple of the nearest-neighbor qubit distance r_0 as shown in **Figure 2**. r_0 is the reference spacing and it is set to 180 nm , corresponding to the value used to extract

the control sequence of the two-qubit gate, that is, $\sqrt{i\text{SWAP}}$, in this study.^[11]

The interaction between qubits is mediated by the long range dipole–dipole interaction between the two electric dipoles at the qubit sites electrically induced by the displacement of the electron of each donor atom toward the interface.^[8]

Assuming identical flip-flop qubits with indexes i and j , the Hamiltonian of the two-qubit system \hat{H}_2^{ij} is the sum of the two single-qubit Hamiltonians \hat{H} (Equation (2)) and the interaction term

$$\hat{H}_2^{ij} = \hat{H}^i \otimes \hat{1} + \hat{1} \otimes \hat{H}^j + \hat{H}_{\text{int}}^{ij} \quad (8)$$

where

$$\hat{H}_{\text{int}}^{ij} = \frac{1}{4\pi\epsilon_0\epsilon_r r^3} \left[\mathbf{p}_i \cdot \mathbf{p}_j - \frac{3(\mathbf{p}_i \cdot \mathbf{r})(\mathbf{p}_j \cdot \mathbf{r})}{r^2} \right] \quad (9)$$

is the dipole–dipole interaction. Here, ϵ_0 is the vacuum permittivity, ϵ_r is the material dielectric constant (equals to 11.7 for silicon), \mathbf{r} is the vector distance between the two qubits and $\mathbf{p}_{i(j)} = \frac{e\hbar}{2} (\hat{1}_{i(j)} + \hat{\sigma}_{z,i(j)})$ is the dipole operator of the qubit to whom is associated the position operator

$$\hat{\sigma}_z^{id} = \frac{d}{\hbar\epsilon_0} \Delta E_z \hat{\sigma}_z + \frac{V_t}{\epsilon_0} \hat{\sigma}_x \quad (10)$$

whose eigenstates $|i\rangle$ and $|d\rangle$ indicate if the electron is localized near the interface or the donor, respectively.

In the following, the effects of the unwanted interactions between qubits on the gate infidelity when two one-qubit gates are applied in parallel are considered. The study is performed taking into account two active qubits separated by none, one, two and three idling qubits.

The operations studied in this section are the $R_z(-\frac{\pi}{2})$ and $R_x(-\frac{\pi}{2})$ rotations which will be applied individually on each qubit. Like in ref. [11], the entanglement fidelity $F^{[20]}$ is calculated for each gate when the $1/f$ noise model on the electric field ΔE_z is considered.^[21–26]

The entanglement fidelity is a figure of merit that does not depend on the initial condition chosen for the qubit and is given by

$$F = \text{tr}[\rho^{\text{RS}} \mathbb{1}_R \otimes (U_i^{-1} U_d)_S \rho^{\text{RS}} \mathbb{1}_R \otimes (U_d^{-1} U_i)_S] \quad (11)$$

where U_i (U_d) is the ideal (disturbed) quantum gate and $\rho^{\text{RS}} = |\psi\rangle\langle\psi|$, where $|\psi\rangle$ represents a maximally entangled state in a double state space generated by two identical Hilbert spaces R and S . $|\psi\rangle = \frac{1}{\sqrt{2}}(|00\rangle + |11\rangle)$ for the single qubit gates and $|\psi\rangle = \frac{1}{\sqrt{2}}(|0000\rangle + |1111\rangle)$ for the two-qubit gate.

In the disturbed quantum gate U_d the $1/f$ noise model is included. In this model the power spectral density is inversely proportional to the frequency and is given by $S(\omega) = \alpha_{\Delta E_z}/(\omega t_0)$, where $\alpha_{\Delta E_z}$ is the noise amplitude, that does not depend on ω , and t_0 is the time unit. Following ref. [23] we generated the $1/f$ noise in the frequency domain as

$$n(\omega) = m(\omega)^{-1/2} e^{i\varphi(\omega)} \quad (12)$$

Table 1. Single $R_z(-\frac{\pi}{2})$ gate parameters.

V_t [GHz]	ΔE_{idle} [V m ⁻¹]	ΔE_{int} [V m ⁻¹]	ΔE_{ct} [V m ⁻¹]	τ_1 [ns]	τ_2 [ns]	T [ns]	K
11.29	10 000	1300	290	2	16	0.08	≈ 20

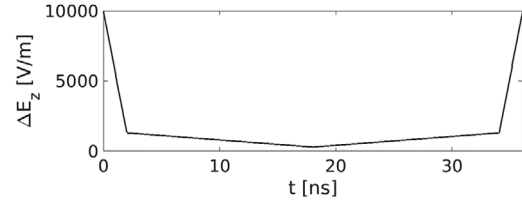


Figure 3. $\Delta E_z(t)$ signal to perform a single $R_z(-\frac{\pi}{2})$ rotation.

where $m(\omega)$ is generated from a standard Gaussian white process and $\varphi(\omega) = [0, 2\pi]$ is a phase factor chosen uniformly. Then, we calculated the inverse Fourier transform and we multiplied the result by $\alpha_{\Delta E_z}$ to obtain the noise in the time domain.

For each gate under study, we generated N instances ($N = 100$) of the $1/f$ charge noise in the time domain to be added to the ideal sequence signals that realize the operation and then we calculate the average over the N resulting entanglement fidelities.

3.1. Parallel R_z Gates

A rotation around the \hat{z} -axis of the Bloch sphere can be obtained by exploiting the phase accumulation between the two qubit states that is generated during the interaction of the system with an external electric field. To do this, a DC electric field $\Delta E_z(t)$ is swept from an idling value ΔE_{idle} , where the electron is confined at the interface, to an intermediate value ΔE_{int} in a time τ_1 . Then, a clock transition value for the electric field ΔE_{ct} , where the dephasing rate is minimum,^[8] is reached after a time τ_2 and, after a time T which sets the angle of rotation, the electric field is reset back to the idling value, following backward the previous sequence steps. The parameters used to set a $-\pi/2$ rotation with an adiabatic factor of $K \approx 20$ are calculated following ref. [8] and are shown in Table 1.

The same $\Delta E_z(t)$ is applied in parallel to the two qubits and it is reported in Figure 3 as a function of time.

In order to quantify the combined effects of the inter-qubit distance r and of the $1/f$ noise amplitude $\alpha_{\Delta E_z}$ on two parallel $R_z(-\frac{\pi}{2})$ gates, the infidelities 1-F are presented in the equi-infidelity graph of Figure 4 for r ranging from r_0 to $4r_0$ and for an $\alpha_{\Delta E_z}$ range spaced between 1 and 1000 V m⁻¹.

A lower infidelity is generally obtained for $r > r_0$ and for smaller $\alpha_{\Delta E_z}$. The worst infidelities are obtained for $r = r_0$ and for high $\alpha_{\Delta E_z}$. When $r = r_0$, the high values of 1-F are due to the long-range inter-qubit dipole–dipole interaction that is sufficiently strong to compromise the nearby parallel operation, while for $r \geq 2r_0$, the inter-qubit distance is enough to reduce the qubits interaction leaving practically unaffected the parallel operations. When $\alpha_{\Delta E_z}$ is increased, 1-F increases up to exceed 10^{-2} when $\alpha_{\Delta E_z} = 100 \text{ V m}^{-1}$ for $r \geq 2r_0$.

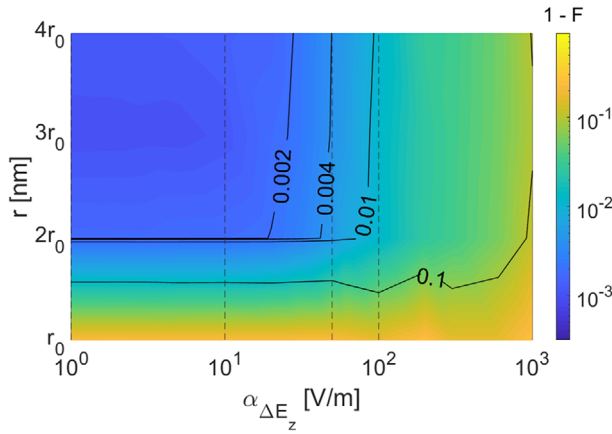


Figure 4. Entanglement infidelity for parallel one-qubit operation $R_z(-\frac{\pi}{2}) \otimes R_z(-\frac{\pi}{2})$ as a function of noise amplitude $\alpha_{\Delta E_z}$ and r . Infidelity is mostly deteriorated in the region close to $r = r_0$ due to a stronger dipole–dipole interaction and where $\alpha_{\Delta E_z}$ is higher. The dashed vertical lines highlight the $\alpha_{\Delta E_z}$ values investigated in the next figure.

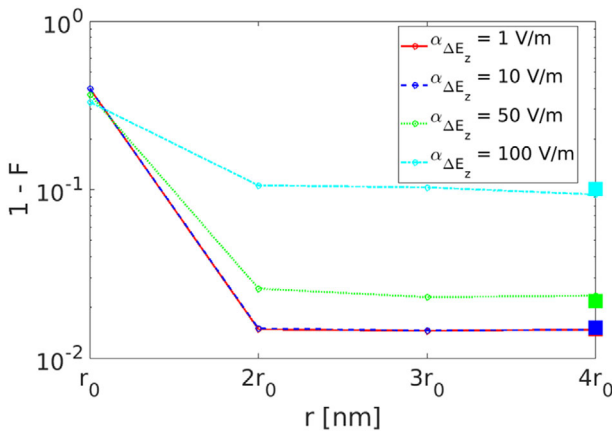


Figure 5. Entanglement infidelity for parallel one-qubit operation $R_z(-\frac{\pi}{2}) \otimes R_z(-\frac{\pi}{2})$ as a function of r for different noise amplitudes $\alpha_{\Delta E_z}$. When $r \geq 2r_0$, the dipole–dipole interaction strength is essentially negligible thus the 1-F curves are flat. The squares represent the infidelity of two non-interacting qubits for each value of $\alpha_{\Delta E_z}$.

In **Figure 5** the effect of the qubits distance on the infidelities of two parallel $R_z(-\frac{\pi}{2})$ gates is shown for different significant values of $\alpha_{\Delta E_z}$ equal to 1, 10, 50, and 100 V m^{-1} . The long range dipole–dipole interaction strength causes the 1-F curves maximum value at $r = r_0$ while the infidelities are almost flat due a reduced interaction for $r \geq 2r_0$. More in detail, we observe that an infidelity minimum, slightly below the infidelity value for non-interacting qubits, appears at $3r_0$ for small $\alpha_{\Delta E_z}$ values (1 and 10 V m^{-1}). In the $r \geq 2r_0$ region the main contribution to the fidelity deterioration is due to $\alpha_{\Delta E_z}$. We point out that the fidelity reaches 99.9% in correspondence to $\alpha_{\Delta E_z} \leq 10 \text{ V m}^{-1}$, 99.6% for $\alpha_{\Delta E_z} = 50 \text{ V m}^{-1}$, and 99% for $\alpha_{\Delta E_z} = 100 \text{ V m}^{-1}$. For comparison, the squares highlighting the infidelity of two non-interacting qubits for each value of $\alpha_{\Delta E_z}$ in the corresponding color are added.

Table 2. Single $R_x(-\frac{\pi}{2})$ gate parameters.

V_i	ΔE_{idle}	ΔE_{int}	ΔE_{ct}	τ_1	τ_2	T	$\max(E_{\text{ac}}(t))$	$T_{E_{\text{ac}}}^{\text{Start}}$	$T_{E_{\text{ac}}}^{\text{ON}}$	K
[GHz]	[V m^{-1}]	[V m^{-1}]	[V m^{-1}]	[ns]	[ns]	[ns]	[V m^{-1}]	[ns]	[ns]	
11.5	10 000	1300	0	2	4	90.5	180	25	40	≈ 20

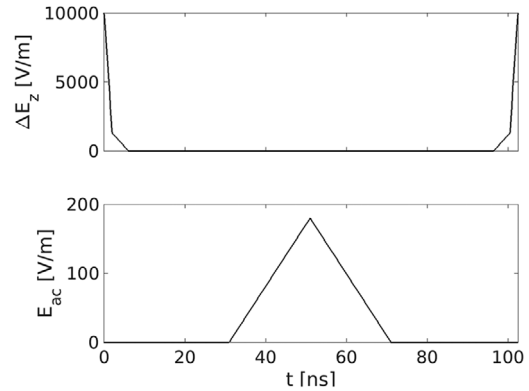


Figure 6. $\Delta E_z(t)$ signal and the time-dependent drive amplitude $E_{\text{ac}}(t)$ to perform a single $R_x(-\frac{\pi}{2})$ operation.

3.2. Parallel R_x Gates

Unlike R_z , a R_x gate needs the addition to the DC electric field of an AC electric field

$$E_a(t) = E_{\text{ac}}(t)\cos(2\pi\epsilon_{\text{ff}}t) \quad (13)$$

in resonance with the flip-flop qubit transition frequency at ΔE_{ct} , where $E_{\text{ac}}(t)$ is the electric field amplitude with a triangular envelope which drives the rotation around the $\hat{x}(\hat{y})$ -axis, ϵ_{ff} is the flip-flop qubit transition frequency associated to the qubit states energy difference and the electric field phase $\phi = 0$. The oscillating field is summed to the DC component after a time $T_{E_{\text{ac}}}^{\text{Start}}$ for a duration $T_{E_{\text{ac}}}^{\text{ON}}$. The parameters shown in **Table 2** are used to obtain a $-\pi/2$ rotation with an adiabatic factor of $K \approx 20$.

For completeness, both the applied $\Delta E_z(t)$ and the time-dependent drive amplitude $E_{\text{ac}}(t)$ as a function of time are reported in **Figure 6**.

Similarly to the case of two parallel \hat{z} -axis rotations, the infidelities of two parallel $R_x(-\frac{\pi}{2})$ gates are studied. The results of **Figure 7** show the 1-F results as a function of the inter-qubit distance r and of the noise amplitude $\alpha_{\Delta E_z}$.

As seen in **Figure 4**, the parallel operations are compromised by the long-range dipole–dipole interaction when $r = r_0$ while infidelity is kept low for $r \geq 2r_0$. In this region 1-F is more affected by the noise and its amplitude increase can raise 1-F up to exceed 10^{-1} when $\alpha_{\Delta E_z} = 100 \text{ V m}^{-1}$. Note that the values of the $R_x(-\frac{\pi}{2}) \otimes R_x(-\frac{\pi}{2})$ infidelity plateaus are higher than those of $R_z(-\frac{\pi}{2}) \otimes R_z(-\frac{\pi}{2})$ for the same $\alpha_{\Delta E_z}$.

Then, the effect of the inter-qubits distance r on the infidelity of two parallel $R_x(-\frac{\pi}{2})$ gates is illustrated in **Figure 8** for four different values of $\alpha_{\Delta E_z}$. Like in **Figure 5**, the infidelities reach their maximum at $r = r_0$, while for $r \geq 2r_0$ the infidelities are only deteriorated by the increase of $\alpha_{\Delta E_z}$. The fidelity reaches 99% in

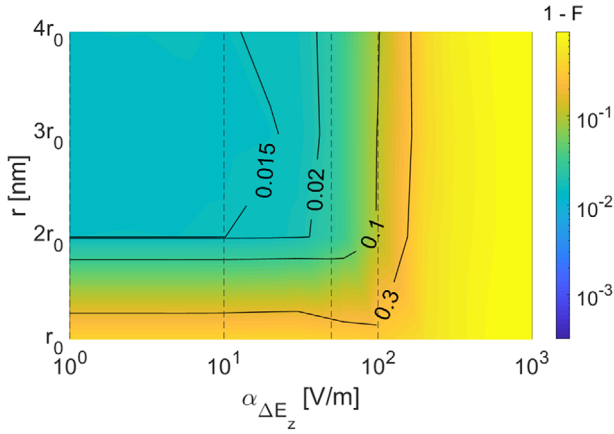


Figure 7. Entanglement infidelity for the operation $R_x(-\frac{\pi}{2}) \otimes R_x(-\frac{\pi}{2})$ as a function of noise amplitude $\alpha_{\Delta E_z}$ and r . Like in $R_z(-\frac{\pi}{2}) \otimes R_z(-\frac{\pi}{2})$ case, the infidelity is deteriorated when $r = r_0$ and for high values of $\alpha_{\Delta E_z}$. The dashed vertical lines highlight the $\alpha_{\Delta E_z}$ values investigated in the next figure.

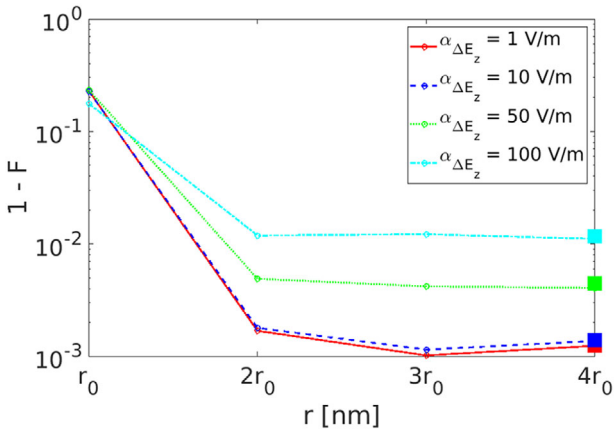


Figure 8. Entanglement infidelity for the operation $R_x(-\frac{\pi}{2}) \otimes R_x(-\frac{\pi}{2})$ calculated as a function of r for different noise amplitudes $\alpha_{\Delta E_z}$. Except for $r < 2r_0$, the curves are predominantly influenced by $\alpha_{\Delta E_z}$. The squares represent the infidelity of two noninteracting qubits for each value of $\alpha_{\Delta E_z}$.

correspondence to $\alpha_{\Delta E_z} \leq 10 \text{ V m}^{-1}$ and drops up to 90% for $\alpha_{\Delta E_z} = 100 \text{ V m}^{-1}$.

4. Parallel Two-Qubit Gate: $\sqrt{i\text{SWAP}}$

In this section the parallel application of two two-qubit operations are studied following the scheme shown in **Figure 9**.

A $\sqrt{i\text{SWAP}}$ gate on a qubit couple is achieved between two donors spaced by $r_0 = 180 \text{ nm}$. First, a DC electric field is applied to both qubits q_i and q_j and finally two identical corrective single R_z gates manipulate the qubits one by one, while the other is kept in an idling state.^[11] All the parameters are reported in **Table 3** and the $\Delta E_z(t)$ signal applied in parallel to both pairs of qubit is shown in **Figure 10**.

In order to study the four-qubit system i, j, k, l , its Hamiltonian \hat{H}_4^{ijkl} which, similarly to the two-qubit system, is obtained as the

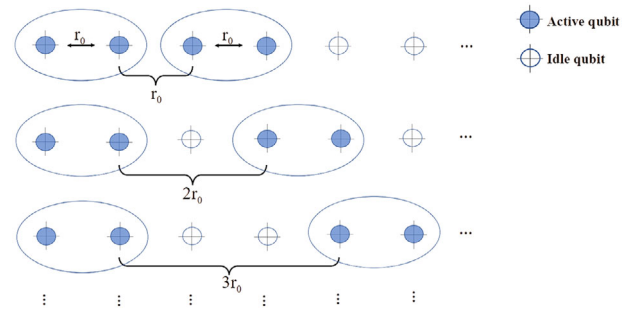


Figure 9. Scheme of a linear array of flip-flop qubits for three example cases when two parallel two-qubit gates are considered. The distance between the qubits operated by two-qubit gate is r_0 . The first couple of qubits is separated from the second couple by a distance r , integer multiple of r_0 .

Table 3. Single $\sqrt{i\text{SWAP}}$ gate parameters.

	V_t [GHz]	ΔE_{idle} [V m ⁻¹]	ΔE_{int} [V m ⁻¹]	ΔE_{ct} [V m ⁻¹]	τ_1 [ns]	τ_2 [ns]	T [ns]	K
q_i, q_j	11.58	10 000	1300	0	1.3	195	2	≈ 20
$q_i, (q_j)$	11.58	10 000	1300	0	2	4	4.5	≈ 33

sum of the two-qubit Hamiltonians \hat{H}_2^{ij} (Equation (8)) and the interaction term (Equation (9)) between only the first nearest neighbors qubits (j and k) and neglecting the others, is expressed by

$$\hat{H}_4^{ijkl} = \hat{H}_2^{ij} \otimes \hat{1}_2 + \hat{1}_2 \otimes \hat{H}_2^{kl} + \hat{1} \otimes \hat{H}_{\text{int}}^{jk} \otimes \hat{1} \quad (14)$$

where $\hat{1}_2$ is the identity matrix in the Hilbert space of two flip-flop qubits.

The infidelities trends of two parallel $\sqrt{i\text{SWAP}}$ gates are shown in **Figure 11** as a function of the distance r and of the noise amplitude $\alpha_{\Delta E_z}$. Similarly to the two parallel one-qubit gates, the infidelity reaches its maximum at $r = r_0$, while for $r \geq 2r_0$, the noise amplitude dominates the behavior of 1-F, which exceeds 10^{-1} when $\alpha_{\Delta E_z} > 100 \text{ V m}^{-1}$.

Finally, the effect of the inter-qubit distance r on 1-F is presented in **Figure 12** for different values of $\alpha_{\Delta E_z}$. The infidelities reach their maximum values at $r = r_0$ where the dipole-dipole interaction between the second and third qubits has the highest impact, while for $r \geq 2r_0$ the 1-F increases only by a $\alpha_{\Delta E_z}$ rise due to a negligible interaction between the qubit couples. The fidelity varies from a maximum value of 99.9% to 90% when $\alpha_{\Delta E_z}$ increases. In particular a curve minimum at $r = 3r_0$ can be observed when $\alpha_{\Delta E_z} = 1, 10 \text{ V m}^{-1}$ whereas no evident minimum results for higher noise levels.

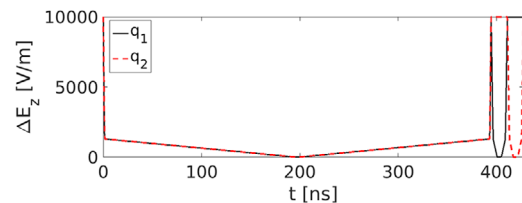


Figure 10. $\Delta E_z(t)$ signal to perform a single $\sqrt{i\text{SWAP}}$.

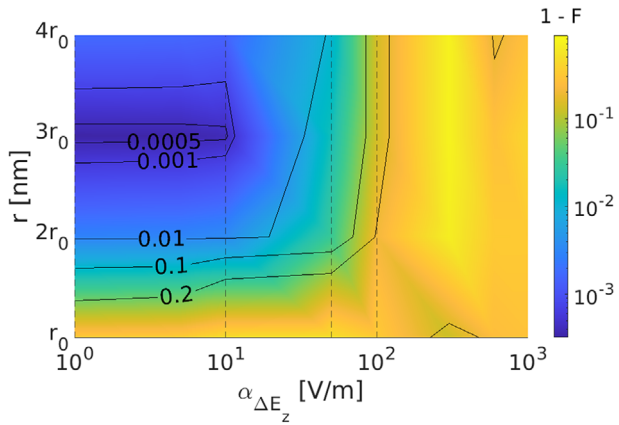


Figure 11. Entanglement infidelity for the operation $\sqrt{i\text{SWAP}} \otimes \sqrt{i\text{SWAP}}$ as a function of noise amplitude $\alpha_{\Delta E_z}$ and r . The infidelity has its highest values when the dipole–dipole interaction between the qubits q_2 and q_3 is stronger and where $\alpha_{\Delta E_z}$ is higher. The nonmonotonic infidelity behavior for increasing $\alpha_{\Delta E_z}$ greater than 300 V m^{-1} is due to statistical errors. The dashed vertical lines highlight the $\alpha_{\Delta E_z}$ values investigated in the next figure.

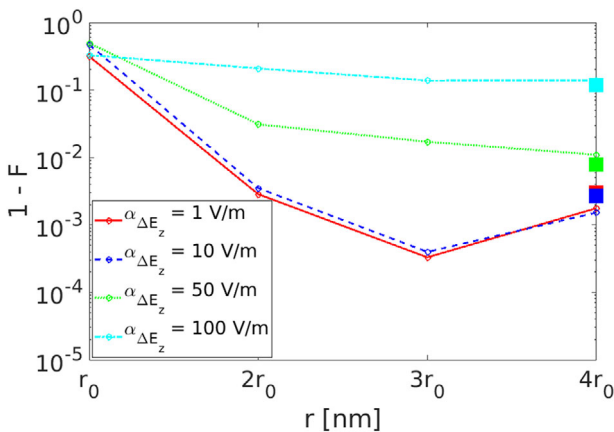


Figure 12. Entanglement infidelity for the operation $\sqrt{i\text{SWAP}} \otimes \sqrt{i\text{SWAP}}$ calculated as a function of r for different noise amplitudes $\alpha_{\Delta E_z}$. Similarly to the two parallel one-qubit gates, when $r \geq 2r_0$, the curves are predominantly influenced by $\alpha_{\Delta E_z}$. The squares represent the infidelity of two non-interacting couples of qubits for each value of $\alpha_{\Delta E_z}$.

The presence of an infidelity minimum around $3r_0$ for small $\alpha_{\Delta E_z}$ with a infidelity value considerably below the noninteracting qubits one is an unexpected result that requires further investigations. It is linked to the complex dynamics of a four qubit system, with first neighbors interacting qubits driven to perform two parallel $\sqrt{i\text{SWAP}}$ gates. It is worth recalling that each couple of qubits is manipulated with a $\sqrt{i\text{SWAP}}$ sequence that, for a given adiabatic factor value, has been optimized to control only a single couple of qubits. Differently from the single one- and two- qubit operations, the adiabatic factor of the parallel control sequence is not controlled thus not kept to a same constant value for different r . We suppose that this reduction in the infidelity value is due to an increase of the adiabatic factor of the two parallel $\sqrt{i\text{SWAP}}$ sequence at $r=3r_0$.

No straightforward conclusions on a monotonic decreasing behavior of the infidelity of two parallel two-qubit operations as a function of r can be inferred. The simulation results show that for $r > 3r_0$ the infidelity of the parallel operations raises, approaching that one of two noninteracting couples of qubits (represented by the squares in Figure 12) because the dipole–dipole interaction between the qubit couples is almost negligible for large r . For $r < 3r_0$ the two couples of qubits are too close and their unwanted coupling is strongly detrimental for the fidelity of the parallel gates.

5. Conclusions

In this work the infidelity of two parallel R_z , R_x and $\sqrt{i\text{SWAP}}$ gates applied on flip-flop qubits arranged in a linear array are studied. The detrimental effects on the entanglement gate infidelity due to the mutual qubit interference and to the $1/f$ noise are taken into account. The results obtained show a greater robustness of $R_z(-\frac{\pi}{2}) \otimes R_z(-\frac{\pi}{2})$ to the noise with respect to the other two parallel operations.

Moreover, a minimum inter-qubit distance $r_{\min} = 2r_0$ for each considered gate can identify a safe region for $r \geq r_{\min}$ where high-fidelity parallel gates can be achieved. In this safe region, the three operations considered in this study show a good robustness to the $1/f$ noise until a noise amplitude of 50 V m^{-1} , with corresponding infidelities roughly below 10^{-1} . Out of the safe region, at $r = r_0$, it is evident that the fidelity deterioration prevents the application of parallel gates.

All the presented results have been obtained by considering qubits with all the same features and driven with the same control sequences taken from ref. [11]. If this hypothesis is removed some strategies to mitigate the unwanted coupling effects between qubits operated in parallel can be applied. In fact by using different sequences with similar adiabatic factors to perform the same three operations, the \hat{H}_{int} terms can be reduced by acting on the coupling rate between qubit operated in parallel. This means increasing the charge qubit energies ϵ_0 and reducing the V_t tunneling couplings. All those results have been obtained by neglecting the effects of the idle qubits placed near and/or between the active ones. Future studies will include those detrimental effects along with mitigation strategies based on a careful reduction of the inter-qubit coupling between idle and active qubits.

Moreover a substantial gate fidelity increase can be expected by exploiting more sophisticated signal sequences obtained from optimal control theory-based methods as done in ref. [27] with a numerical calculation based on a simplex method mixed with a genetic algorithm in a double-dot hybrid qubit and in ref. [28] where a GRAPE (gradient ascent pulse engineering) optimal control method was implemented on donor electron spin qubits in Si semiconductors.

It is recognized that is fundamental for quantum computation not only a small gate time with respect to the qubit coherence time but also a sufficiently high level of parallelism. As a first approximation, the results obtained for two parallel operations on two qubits (two couples of qubits) can be extended to an arbitrary number of parallel operated qubits (couples of qubits). The resulting $r_{\min} = 2r_0$ implies that at least an idle qubit is needed between two active ones to retain high-fidelity parallel one-qubit gates. Nevertheless, one-qubit gates can be executed anyway by

applying a serialization of their control sequences in two consecutive steps: in the first one, qubits with odd (even) array indexes are operated in parallel and then, in the second step, the even (odd) indexed qubits are manipulated in parallel. A similar consideration can be done for the serialization of parallel two-qubit gates: in the first time step, a set of qubit couples selected in such a way to leave an idle couple between the two active ones are operated and then, during the second time step, the qubit couples that were idling during the first step are manipulated and the remaining ones are left in idle. Surely this leads to a one- (two-) logical qubit gate time that are two times longer than the one- (two-) qubit gate duration but it represents a useful scheme that allows the parallelization of quantum gate operations in view of the realization and exploitation of quantum error correction circuits.

Acknowledgements

Open Access Funding provided by Consiglio Nazionale delle Ricerche within the CRUI-CARE Agreement.

Conflict of Interest

The authors declare no conflict of interest.

Data Availability Statement

The data that support the findings of this study are available from the corresponding author upon reasonable request.

Keywords

1/f noise, donor qubit, flip-flop qubit, parallel quantum gate, qubit array

Received: October 25, 2021

Revised: January 4, 2022

Published online: January 27, 2022

[1] B. E. Kane, *Nature* **1998**, 393, 133.

[2] J. P. Gordon, K. D. Bowers, *Phys. Rev. Lett.* **1958**, 1, 368.

[3] G. Feher, E. A. Gere, *Phys. Rev.* **1959**, 114, 1245.

- [4] A. M. Tyryshkin, S. Tojo, J. J. L. Morton, H. Riemann, N. V. Abrosimov, P. Becker, H.-J. Pohl, T. Schenkel, M. L. W. Thewalt, K. M. Itoh, S. A. Lyon, *Nat. Mater.* **2012**, 11, 143.
- [5] M. Steger, K. Saeedi, M. L. W. Thewalt, J. J. L. Morton, H. Riemann, N. V. Abrosimov, P. Becker, H.-J. Pohl, *Science* **2012**, 336, 1280.
- [6] K. Saeedi, S. Simmons, J. Z. Salvail, P. Dluhy, H. Riemann, N. V. Abrosimov, P. Becker, H.-J. Pohl, J. J. L. Morton, M. L. W. Thewalt, *Science* **2013**, 342, 830.
- [7] A. Morello, J. J. Pla, P. Bertet, D. N. Jamieson, *Adv. Quantum Technol.* **2020**, 3, 2000005.
- [8] G. Tosi, F. A. Mohiyaddin, V. Schmitt, S. Tenberg, R. Rahman, G. Klimeck, A. Morello, *Nat. Commun.* **2017**, 8, 450.
- [9] G. Tosi, F. A. Mohiyaddin, S. Tenberg, A. Laucht, A. Morello, *Phys. Rev. B* **2018**, 98, 075313.
- [10] F. A. Calderon-Vargas, E. Barnes, S. E. Economou, *arXiv:2101.11592v1* **2021**.
- [11] E. Ferraro, D. Rei, M. Paris, M. De Michielis, *EPJ Quantum Technol.* **2022**, 9, 2.
- [12] A. M. Steane, *Phys. Rev. Lett.* **1996**, 77, 793.
- [13] R. Yousefjani, A. Bayat, *Quantum* **2021**, 5, 460.
- [14] C. Figgatt, A. Ostrander, N. M. Linke, K. A. Landsman, D. Zhu, D. Maslov, C. Monroe, *Nature* **2019**, 572, 368.
- [15] C. Song, K. Xu, W. Liu, C. ping Yang, S.-B. Zheng, H. Deng, Q. Xie, K. Huang, Q. Guo, L. Zhang, P. Zhang, D. Xu, D. Zheng, X. Zhu, H. Wang, Y.-A. Chen, C.-Y. Lu, S. Han, J.-W. Pan, *Phys. Rev. Lett.* **2017**, 119, 180511.
- [16] T. Olsacher, L. Postler, P. Schindler, T. Monz, P. Zoller, L. M. Sieberer, *PRX Quantum* **2020**, 1, 020316.
- [17] K. A. Landsman, Y. Wu, P. H. Leung, D. Zhu, N. M. Linke, K. R. Brown, L. Duan, C. Monroe, *Phys. Rev. A* **2019**, 100, 022332.
- [18] H. Levine, A. Keesling, G. Semeghini, A. Omran, T. T. Wang, S. Ebadi, H. Bernien, M. Greiner, V. Vuletić, H. Pichler, M. D. Lukin, *Phys. Rev. Lett.* **2019**, 123, 170503.
- [19] J. Simon, F. A. Calderon-Vargas, E. Barnes, S. E. Economou, *Phys. Rev. B* **2020**, 101, 205307.
- [20] M. A. Nielsen, I. L. Chuang, *Quantum Computation and Quantum Information*, Cambridge University Press, Cambridge **2000**.
- [21] E. Paladino, Y. M. Galperin, G. Falci, B. L. Altshuler, *Rev. Mod. Phys.* **2014**, 86, 361.
- [22] J. M. Epstein, A. W. Cross, E. Magesan, J. M. Gambetta, *Phys. Rev. A* **2014**, 89, 062321.
- [23] X. Yang, X. Wang, *Sci. Rep.* **2016**, 6, 28996.
- [24] C. Zhang, R. E. Throckmorton, X. C. Yang, X. Wang, E. Barnes, S. Das-Sarma, *Phys. Rev. Lett.* **2017**, 118, 216802.
- [25] Y.-C. Yang, S. N. Coppersmith, M. Friesen, *Phys. Rev. A* **2019**, 100, 022337.
- [26] E. Ferraro, M. De Michielis, *Sci. Rep.* **2020**, 10, 17780.
- [27] E. Ferraro, M. De Michielis, M. Fanciulli, E. Prati, *Quantum Inf. Process.* **2015**, 14, 47.
- [28] D.-B. Tsai, P.-W. Chen, H.-S. Goan, *Phys. Rev. A* **2009**, 79, 060306(R).